Blind Proximal Diffusion Model for Joint Image and Sensitivity Estimation in Parallel MRI

Xing Li[1], Yan Yang[1(✉)], and Hairong Zheng[2] Zongben Xu[1]

[1] Xian Jiaotong University, Xian, China
{listar0810,yangyan,zbxu}@mail.xjtu.edu.cn
[2] Shenzhen Advanced Technology Research Institute, Chinese Academy of Sciences, Shenzhen, China
hr.zheng@siat.ac.cn

Abstract. Parallel imaging (PI) has demonstrated notable efficiency in accelerating magnetic resonance imaging (MRI) using deep learning techniques. However, these models often face challenges regarding their adaptability and robustness across varying data acquisition. In this work, we introduce a novel joint estimation framework for MR image reconstruction and multi-channel sensitivity maps utilizing denoising diffusion models under blind settings, termed Blind Proximal Diffusion Model in Parallel MRI (BPDM-PMRI). BPDM-PMRI formulates the reconstruction problem as a non-convex optimization task for simultaneous estimation of MR images and sensitivity maps across multiple channels. We employ the proximal alternating linearized minimization (PALM) to iteratively update the reconstructed MR images and sensitivity maps. Distinguished from the traditional proximal operators, our diffusion-based proximal operators provide a more generalizable and stable prior characterization. Once the diffusion model is trained, it can be applied to various sampling trajectories. Comprehensive experiments conducted on publicly available MR datasets demonstrate that BPDM-PMRI outperforms existing methods in terms of denoising effectiveness and generalization capability, while keeping clinically acceptable inference times.

Keywords: Magnetic Resonance Imaging · Parallel MR Imaging · Diffusion Model · Proximal Operator Learning.

1 Introduction

Magnetic Resonance Imaging (MRI) is a widely employed non-invasive technique for clinical diagnosis. However, its extended acquisition time in k-space poses limitations such as patient discomfort and motion-related artifacts, restricting its clinical applications. To address this limitation, parallel imaging (PI) and compressive sensing (CS) techniques have emerged to accelerate MRI.

PI reduces the required k-space data samples by encoding sensitivity maps of multiple coils [8], while CS-MRI reconstructs MRI images by exploiting sparsity in the k-space through sparse sampling [16]. Combining these techniques, known as CS-PI, further accelerates MRI [10]. CS-PI methods are classified into

explicit-calibration, auto-calibration, and calibration-less methods [23]. Explicit-calibration relies on estimating coil sensitivity maps from pre-scanning calibration images [18, 2, 15]. However, misalignment between scans can lead to sensitivity miscalibration errors, degrading image quality. To address this issue, auto-calibration methods [8, 17, 22, 9] extract auto-calibration signals (ACS) from the central region of fully-sampled k-space to alleviate miscalibration errors. However, their reconstruction accuracy heavily depends on the accuracy of the estimated sensitivity profile, especially when only a limited number of ACS lines are available at high acceleration rates. Calibration-less methods reconstruct multi-channel k-space data directly without calibration. They synthesize the final MR image using the square root of the sum of squares of the reconstructed images [21, 14, 10]. However, these methods face high computational complexity. Recently, deep learning has proven effective for solving inverse problems, including parallel MR imaging. These methods employ deep neural networks to directly map under-sampled k-space data to aliasing-free images [25]. Nonetheless, they ofen lack specific domain knowledge of the CS-PI mechanism. To overcome this limitation, recent approaches such as incorporating imaging models or data consistency of k-space into the network have been proposed [6, 19]. Additionally, explicit-calibration CS-PI methods such as [11, 1] learn de-aliasing networks or Fields of Experts (FoE) models through gradient descent procedures, estimating sensitivity maps via calibration using ESPIRiT [22]. Despite their promising results and speed, they require separate estimation of coil sensitivity maps. Moreover, Yang *et al.* [24] proposed an iterative deep learning-based method for CS-PI to jointly estimate MR images and coil sensitivities, even with high acceleration factors or fewer ACS lines in k-space.

More recently, unsupervised deep learning methods, particularly generative models, have shown great potential in learning complex prior distributions and have advantages in alleviating the limitations of learning flexibility. For instance, Chung *et al.* [7] introduced a score-POCS model for solving inverse problems in imaging by leveraging the learned score function as a prior. However, denoising diffusion processes have a tendency to alter the original distribution of the target image due to the randomness of noise. Consequently, denoising diffusion methods often overlook the consistency of anatomical structures in medical images, resulting in clinically less relevant outcomes. Additionally, current diffusion-based CS-PI methods primarily focus on MR image denoising without considering sensitivity maps. In this work, we introduce a novel Blind Proximal Diffusion Model in Parallel MRI (BPDM-PMRI) for reconstructing MR images from under-sampled k-space measurements. Our main contributions include:

- We propose a joint optimization approach for blind parallel MRI reconstruction, which incorporates denoising diffusion probabilistic models for images and sensitivity maps. To the best of our knowledge, this is the first diffusion-based model for blind CS-PI.
- We employ the PALM [4] algorithm to solve the blind CS-PI model and substitute regularizers with off-the-shelf diffusion models, serving as denoising priors to approximate the global optimal solution.

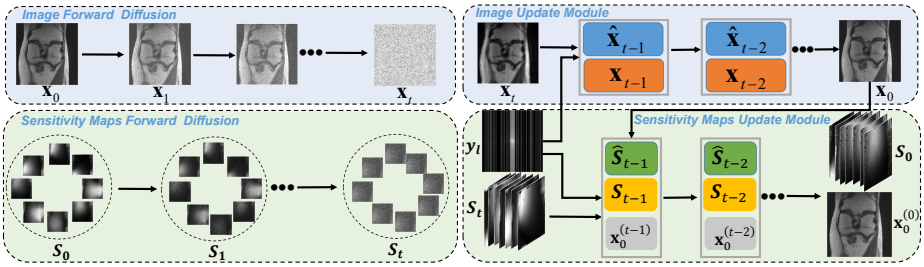

Fig. 1. Schematic diagram of BPDM-PMRI. MR image and sensitivity maps diffusion models are trained during the forward process. In the Image Update Module (**IUM**), sampling from the image diffusion model with the start of the under-sampled MR images $\mathbf{x}_t$, then updating with $\hat{\mathbf{x}}_{t-1}$ and $\mathbf{x}_{t-1}$ until the final sample $\mathbf{x}_0$. Next, sampling from the sensitivity maps diffusion model with the start of the estimated sensitivity maps $\mathbf{S}_t$, then updating with $\hat{\mathbf{S}}_{t-1}$, $\mathbf{S}_{t-1}$, and $\mathbf{x}_0^{(t-1)}$ until the final sensitivity maps $\mathbf{S}_0$ and reconstructed MR image $\mathbf{x}_0^{(0)}$. The under-sampled k-space measurements y_l participates in the iterations of two modules.

- We improve sampling speed significantly by utilizing diffusion models derived from initial images and sensitivity maps and sampling images and sensitivity maps within 120 steps, resulting in a remarkable 16.6× speedup.
- We present a novel alternating optimization scheme between updated images and sensitivity maps, which provides informative guidance for MR reconstruction and accelerates model convergence. This technique proves to be highly promising for clinical applications.

2 Methodology

We consider the reconstruction model for blind parallel MR imaging in the following form:

$$\min_{\mathbf{x},\mathbf{S}} E\left(\mathbf{x},\mathbf{S}\right) := H\left(\mathbf{x},\mathbf{S}\right) + \lambda P(\mathbf{x}) + \gamma \sum_{l=1}^{N_c} R\left(\mathbf{s}_l\right), \tag{1}$$

where

$$H\left(\mathbf{x},\mathbf{S}\right) = \frac{1}{2}\sum_{l=1}^{N_c} \|\mathbf{A}\mathbf{s}_l \odot \mathbf{x} - \mathbf{y}_l\|_2^2 + \frac{\alpha}{2}\|\mathbf{x}\|_2^2 + \frac{\beta}{2}\sum_{l=1}^{N_c}\|\mathbf{s}_l\|_2^2 . \tag{2}$$

The first term of $H\left(\mathbf{x},\mathbf{S}\right)$ ensures data consistency among reconstructed MR image $\mathbf{x}$, estimated per-channel sensitivity map $\mathbf{s}_l$ and its under-sampled data $\mathbf{y}_l$ in k-space. The total number of coils is N_c. $\mathbf{A} = \mathbf{MF}$, $\mathbf{F} \in \mathbb{C}^{N\times N}$ denotes the Fourier transform matrix, and $\mathbf{M} \in \mathbb{C}^{M\times N}$ is the sampling matrix in k-space. Minimizing (1) poses a bilinear inverse problem and typically does not

guarantee the existence of a globally optimal solution. In $H(\mathbf{x}, \mathbf{S})$, we include squared ℓ_2 regularization terms of the image $\mathbf{x}$ and sensitivity maps $\mathbf{s}_l$ to transform bi-convex function $\|\mathbf{A}\mathbf{s}_l \odot \mathbf{x} - \mathbf{y}_l\|_2^2$ to a strongly bi-convex function, where α and β are corresponding regularization parameters. $P(\cdot)$ and $R(\cdot)$ are two additional undetermined regularization functions for characterizing the complex priors of MR image and the sensitivity maps respectively, further constraining the solution space. λ and γ are regularization parameters corresponding to the relative weights of the undetermined regularization terms of MR image and the sensitivity maps respectively.

2.1 Model Optimization

Solving (1) can be achieved by iteratively updating variables $\mathbf{x}$ and $\mathbf{S}$, which is equivalent to solving the following subproblem:

$$\begin{aligned} \mathbf{x}^{(k+1)} &\in \underset{\mathbf{x}}{\operatorname{argmin}} H\left(\mathbf{x}, \mathbf{S}^{(k)}\right) + \lambda P(\mathbf{x}), \\ \mathbf{s}_l^{(k+1)} &\in \underset{\mathbf{s}_l}{\operatorname{argmin}} H\left(\mathbf{x}^{(k+1)}, \mathbf{S}\right) + \gamma R(\mathbf{s}_l). \end{aligned} \tag{3}$$

Then H is linearized at points $\mathbf{x}^{(k)}$ and $\mathbf{s}_l^{(k)}$ respectively by the following equations:

$$\begin{aligned} \mathbf{x}^{(k+1)} &\in \underset{\mathbf{x}}{\operatorname{argmin}} \left\langle \mathbf{x} - \mathbf{x}^{(k)}, \nabla_{\mathbf{x}} H\left(\mathbf{x}^{(k)}, \mathbf{S}^{(k)}\right) \right\rangle + \frac{\alpha}{2} \left\| \mathbf{x} - \mathbf{x}^{(k)} \right\|_2^2 + \lambda P(\mathbf{x}), \\ \mathbf{s}_l^{(k+1)} &\in \underset{s_l}{\operatorname{argmin}} \left\langle \mathbf{s}_l - \mathbf{s}_l^{(k)}, \nabla_{\mathbf{s}_l} H\left(\mathbf{x}^{(k+1)}, \mathbf{S}^{(k)}\right) \right\rangle + \frac{\alpha}{2} \left\| \mathbf{s}_l - \mathbf{s}_l^{(k)} \right\|_2^2 + \gamma R\left(\mathbf{s}_l\right), \end{aligned} \tag{4}$$

where

$$\begin{aligned} \nabla_{\mathbf{x}} H\left(\mathbf{x}^{(k)}, \mathbf{S}^{(k)}\right) &= \sum_{l=1}^{N_c} \left[\left(\mathbf{s}_l^{(k)}\right)^* \odot \mathbf{A}^\top \left(\mathbf{A}\mathbf{s}_l^{(k)} \odot \mathbf{x}^{(k)} - \mathbf{y}_l\right) \right] + \alpha \mathbf{x}^{(k)}, \\ \nabla_{\mathbf{s}_l} H\left(\mathbf{x}^{(k+1)}, \mathbf{S}^{(k)}\right) &= \left(\mathbf{x}^{(k+1)}\right)^* \odot \mathbf{A}^\top \left(\mathbf{A}\mathbf{s}_l^{(k)} \odot \mathbf{x}^{(k+1)} - \mathbf{y}_l\right) + \beta \mathbf{s}_l^{(k)}. \end{aligned} \tag{5}$$

$\nabla_{\mathbf{x}} H\left(\mathbf{x}^{(k)}, \mathbf{S}^{(k)}\right)$ and $\nabla_{\mathbf{s}_l} H\left(\mathbf{x}^{(k+1)}, \mathbf{S}^{(k)}\right)$ are gradients of multivariate function H with respect to $\mathbf{x}$ and $\mathbf{s}_l$. $\langle \cdot, \cdot \rangle$ is an inner product operator. The superscripts $*$ and $\top$ represent conjugate and conjugate transpose respectively. Thus the problem of minimizing the sum of a smooth function H with a non-smooth one P or R can be simplified to the following sub-problems:

$$\begin{aligned} \mathbf{x}^{(k+1)} &\in \underset{\mathbf{x}}{\operatorname{argmin}} \frac{1}{2} \left\| \mathbf{x} - \left(\mathbf{x}^{(k)} - \frac{1}{\alpha} \nabla_{\mathbf{x}} H\left(\mathbf{x}^{(k)}, \mathbf{S}^{(k)}\right) \right) \right\|_2^2 + \frac{\lambda}{\alpha} P(\mathbf{x}), \\ \mathbf{s}_l{}^{(k+1)} &\in \underset{\mathbf{s}_l}{\operatorname{argmin}} \frac{1}{2} \left\| \mathbf{s}_l - \left(\mathbf{s}_l{}^{(k)} - \frac{1}{d} \nabla_{\mathbf{s}_l} H\left(\mathbf{x}^{(k+1)}, \mathbf{S}^{(k)}\right) \right) \right\|_2^2 + \frac{\gamma}{d} R\left(\mathbf{s}_l\right). \end{aligned} \tag{6}$$

Using the definition of proximal operator, we obtain the following PALM algorithm [4] at k-th iteration:

$$\begin{aligned}\mathbf{x}^{(k+1)} &\in \operatorname{prox}_{\frac{\lambda}{\alpha}P}\left(\mathbf{x}^{(k)}-\frac{1}{\alpha}\nabla_{\mathbf{x}}H\left(\mathbf{x}^{(k)},\mathbf{S}^{(k)}\right)\right),\\ \mathbf{s}_l{}^{(k+1)} &\in \operatorname{prox}_{\frac{\gamma}{d}R}\left(\mathbf{s}_l{}^{(k)}-\frac{1}{d}\nabla_{\mathbf{s}_l}H\left(\mathbf{x}^{(k+1)},\mathbf{S}^{(k)}\right)\right),\end{aligned} \tag{7}$$

where $l \in \{1,2,\cdots,N_c\}$ and $k \in \{0,1,\cdots,K-1\}$.$\mathbf{S}^{(0)} = \left\{\mathbf{s}_1^{(0)},\mathbf{s}_2^{(0)},\cdots,\mathbf{s}_{N_c}^{(0)}\right\}$ is an initial estimation of sensitivity maps. Each of them, e.g., $\mathbf{s}_l^{(0)}$, can be estimated based on the initial estimation of l-th coil MR image $\mathbf{A}^\top\mathbf{y}_l$ and the reconstructed MR image using SoS: $\mathbf{s}_l{}^{(0)} = \frac{\mathbf{A}^\top\mathbf{y}_l}{\sqrt{\sum_{l=1}^{N_c}(\mathbf{A}^\top\mathbf{y}_l)^*\odot(\mathbf{A}^\top\mathbf{y}_l)}}$, where the denominator is the estimation of MR image by SoS. With $\mathbf{S}^{(0)}$, based on the PI imaging model, $\mathbf{x}^{(0)} = \sum_{l=1}^{N_c}\left(\mathbf{s}_l^{(0)}\right)^*\odot\left(\mathbf{A}^\top\mathbf{y}_l\right)$.

2.2 BPDM-PMRI

It is challenging to efficiently compute the proximal operators corresponding to the regularizers for the MR image and coil sensitivities, *i.e.,* $\operatorname{prox}_{\frac{\lambda}{\alpha}P}$ and $\operatorname{prox}_{\frac{\gamma}{d}R}$. As generative diffusion models provide alternatives for the proximal operators, we substitute the proximal operator $\operatorname{prox}_{\frac{\lambda}{\alpha}P}$ and $\operatorname{prox}_{\frac{\gamma}{d}R}$ by two pretrained diffusion probabilistic model, *i.e.,* MR image restoration operator $R_\theta(\mathbf{x},t)$ and $R_\phi(\mathbf{S},t)$.

$$\begin{aligned}\mathbf{x}^{(k+1)} &= \operatorname{prox}_{\frac{\lambda}{\alpha}P}\left(\tilde{\mathbf{x}}^{(k)}\right) \triangleq R_\theta\left(\widetilde{\mathbf{x}}^{(k)}\right),\\ \mathbf{s}_l^{(k+1)} &= \operatorname{prox}_{\frac{\gamma}{d}R}\left(\tilde{\mathbf{s}_l}^{(k)}\right) \triangleq R_\phi\left(\widetilde{\mathbf{s}_l}^{(k)}\right),\end{aligned} \tag{8}$$

where

$$\begin{aligned}\tilde{\mathbf{x}}^{(k)} &= \mathbf{x}^{(k)}-\eta_{\mathbf{x}}\nabla_{\mathbf{x}}H\left(\mathbf{x}^{(k)},\mathbf{S}^{(k)}\right),\\ \tilde{\mathbf{s}}_l^{(k)} &= \mathbf{s}_l^{(k)}-\eta_{\mathbf{s}}\nabla_{\mathbf{s}_l}H\left(\mathbf{x}^{(k+1)},\mathbf{S}^{(k)}\right).\end{aligned} \tag{9}$$

Our proposed BPDM-PMRI employs diffusion proximal operators to substitute the restoration operators in (8). As shown in Fig. 1, the MR image reconstruction process comprises the Image Update Module (**IUM**) and the Sensitivity Maps Update Module (**SMUM**). The **IUM** iteratively generates MR images using initially estimated sensitivity maps, while the **SMUM** utilizes the MR images generated in the **IUM** to guide sensitivity maps generation and achieve better MR image. Details of these two modules are as follows.

Image Update Module. To integrate the iterative process with the diffusion model, the iteration step is indicated in the subscripts throughout the following process. Given the initial step $t = T_1$ and initialization $\mathbf{x}_t = \mathbf{x}^{(0)}$ of the MR

image, along with the initialization of sensitivity maps $\mathbf{S}^{(0)}$, the MR image $\mathbf{x}$ in the t-th iteration can be updated as follows:

$$\begin{aligned} \hat{\mathbf{x}}_{t-1} &= \frac{1}{\sqrt{\bar{\alpha}_t}}(\mathbf{x}_t + (1-\bar{\alpha}_t)s_\theta(\mathbf{x}_t, t)), \\ \mathbf{x}_{t-1} &= \hat{\mathbf{x}}_{t-1} - \eta_{\mathbf{x}} \nabla_{\mathbf{x}} H\left(\hat{\mathbf{x}}_{t-1}, \mathbf{S}^{(0)}\right), \end{aligned} \tag{10}$$

where $s_\theta(\mathbf{x}_t, t)$ is score function of image with score matching methods. $\bar{\alpha}_t$ is related to the variance of the noise in the image diffusion model. $\nabla_{\mathbf{x}} H\left(\hat{\mathbf{x}}_{t-1}, \mathbf{S}^{(0)}\right)$ can be calculated by (5).

Sensitivity Maps Update Module. Given the starting step $t = T_2$ and $\mathbf{x}_0^{(t)}$ corresponding to the final reconstruction $\mathbf{x}_0$ of the **IUM**, along with the initialization $\mathbf{S}^{(0)}$ of sensitivity maps, the sensitivity maps $\mathbf{s}_l$ of the l-th channel in the t-th iteration is formulated:

$$\begin{aligned} \hat{\mathbf{S}}_{t-1} &= \frac{1}{\sqrt{\bar{\alpha}_t}}(\mathbf{S}_t + (1-\bar{\alpha}_t)s_\theta(\mathbf{S}_t, t)), \\ \mathbf{S}_{t-1} &= \hat{\mathbf{S}}_{t-1} - \eta_s \nabla_{s_l} H\left(\mathbf{x}_0^{(t)}, \hat{\mathbf{S}}_{t-1}\right), \\ \mathbf{x}_0^{(t-1)} &= \mathbf{x}_0^{(t)} - \eta_{\mathbf{x}} \nabla_{\mathbf{x}} H\left(\mathbf{x}_0^{(t)}, \hat{\mathbf{S}}_{t-1}\right), \end{aligned} \tag{11}$$

where $s_\theta(\mathbf{S}_t, t)$ is score function of sensitive maps with score matching methods. $\bar{\alpha}_t$ is related to the variance of the noise in the sensitivity maps diffusion model. $\nabla_{s_l} H\left(\mathbf{x}_0^{(t)}, \hat{\mathbf{S}}_{t-1}\right)$ can be calculated by (5). Generally, the simultaneous update of images and sensitivity maps can facilitate rapid convergence of the images, thereby accelerating the reconstruction speed at this iteration. Finally, we have the reconstructed MR image $\mathbf{x}_0^{(0)}$.

3 Experiments

Datasets and Experimental Setup We conducted training and testing of BPDM-PMRI using in-vivo knee MR data from the NYU dataset. The raw data comprises 15-channel k-space data with a matrix size of 320×320, all acquired without acceleration. We randomly selected 10 slices from each of 55 subjects and finally obtained 350 and 100 multi-channel data as training and test sets. We derived complex-valued ground-truth MR images by synthesizing multichannel images reconstructed from fully-sampled k-space data, utilizing ground-truth sensitivity maps estimated by ESPIRiT with 40 ACS lines. For experiment, we employed 1D Cartesian random masks, a practical mode for CS-PI, with acceleration factors of $R_A = 4$, 6, and 8. The quality assessment of the reconstructed MR images involved measuring the average peak signal-to-noise ratio (PSNR), normalized root mean square error (nRMSE), and structural similarity index measure (SSIM) across the whole test set.

Table 1. Comparison of average reconstruction accuracy at different sampling rates using PSNR (dB), SSIM, and nRMSE

ACC	R_A**=4**			R_A**=6**			R_A**=8**		
Method	PSNR ↑	SSIM ↑	nRMSE ↓	PSNR ↑	SSIM ↑	nRMSE ↓	PSNR ↑	SSIM ↑	nRMSE ↓
Zero-filled	27.4755	0.7235	0.1684	26.7098	0.6897	0.1840	26.0822	0.6711	0.1977
TV	29.7786	0.7061	0.1305	27.9858	0.6531	0.1596	26.7589	0.6209	0.1834
GRAPPA	31.5265	0.7865	0.1072	29.3383	0.7229	0.1369	27.4601	0.6739	0.1691
SPIRiT	32.3176	0.8235	0.0981	29.5908	0.7392	0.1331	27.7948	0.6940	0.1632
AC-LORAKS	32.8592	0.8262	0.0882	30.8367	0.7443	0.1166	28.7277	0.6962	0.1475
Fast-JTV	33.1288	0.8322	0.0895	30.6359	0.7494	0.1188	28.7174	0.7046	0.1476
ENLIVE	33.1474	0.8201	0.0917	30.4342	0.7470	0.1190	28.2173	0.7028	0.1608
LINDBERG	33.9495	0.8516	0.0824	31.0982	0.8203	0.1016	29.0735	0.7480	0.1404
Deep-SLR	**34.8320**	**0.8938**	**0.0737**	31.0806	0.8146	0.1120	29.1012	0.7674	0.1402
DDPM-MRI	31.1729	0.7839	0.1138	29.4611	0.7310	0.1370	28.3047	0.7015	0.1562
BPDM-PMRI	34.3807	0.8915	0.0788	**31.3265**	**0.8210**	**0.1099**	**29.2249**	**0.7741**	**0.1395**

Implementation Details We trained diffusion models for image and sensitivity maps using ground-truth MR images and sensitivity maps. The Adam optimizer was employed with a learning rate of 0.0001 and β values of 0.9 and 0.999. The default noise schedule parameters were adopted from [12]. The training involved 1000 forward diffusion steps and 100 reverse steps for image inference, as well as 20 reverse steps for sensitivity maps inference, with DDIM [20] sampling mode. A single NVIDIA Tesla V100s GPU was used for both training and inference.

Performance Evaluation We compared BPDM-PMRI with seven traditional model-based PI methods, including TV[3], Fast-JTV[5], ENLIVE[13], GRAPPA[8], AC-LORAKS[9], SPIRiT[17], and LINDBERG[23]. TV reconstruction employs iterative algorithms with total variation regularization. GRAPPA, SPIRiT, and AC-LORAKS are auto-calibration methods that are commonly used in clinical settings. Fast-JTV, LINDBERG, and ENLIVE are calibration-less methods. Among them, Fast-JTV and LINDBERG solve reconstruction models with a joint total variation and a dictionary-based joint sparsity regularization on images of multi-coils. ENLIVE simultaneously estimates coil profiles and MR images by solving a nonlinear reconstruction model with predefined regularization terms. Additionally, we evaluated our method against supervised deep learning methods, Deep-SLR, and the diffusion model of DDPM-MRI.

Table 1 presents the quantitative accuracy of various reconstruction techniques using 1D Cartesian random masks with acceleration factors R_A of 4, 6, and 8. Compared to model-based approaches like GRAPPA, SPIRiT, AC-LORAKS, Fast-JTV, and ENLIVE, our proposed method exhibits superior reconstruction accuracy across all three acceleration factors. Notably, our network outperforms these traditional methods and DDPM-MRI by an average at least 2 dB. When compared to the supervised deep learning method, Deep-SLR, our approach achieves the best reconstruction performance at acceleration factors of $R_A = 6$ and 8. Our method iteratively updates sensitivity maps and MR

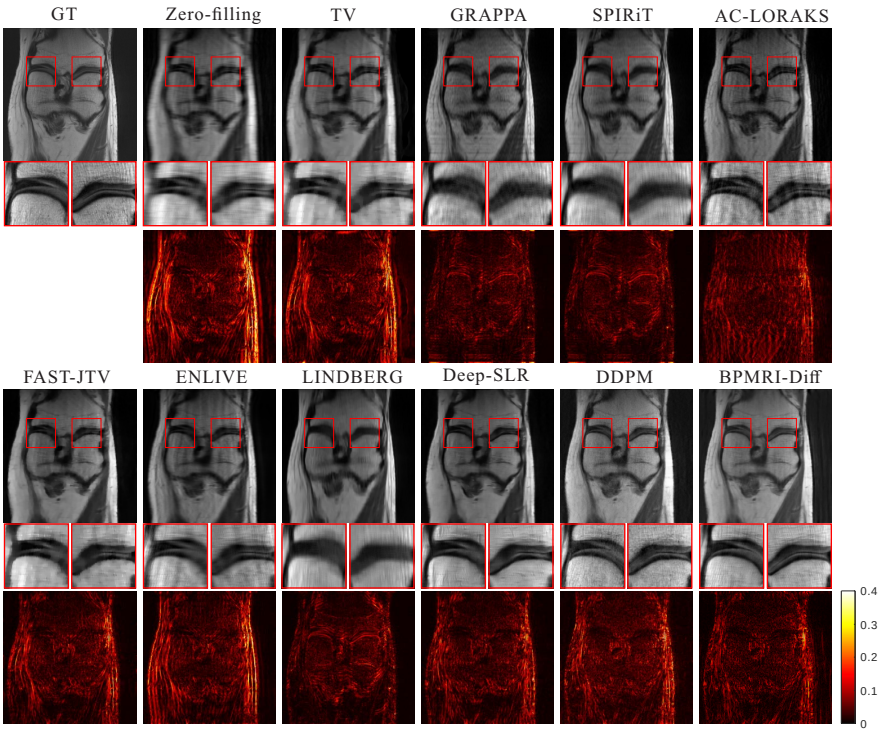

Fig. 2. Examples of reconstructed knee images using an uniform mask at $R_A = 6$.

images using the diffusion proximal operator, leading to enhanced performance in an unsupervised manner. In addition to quantitative evaluations, Fig. 2 provides visual comparisons of reconstructed images under 6× acceleration using a random mask. Our proposed method produces high-quality images with no noticeable artifacts and richer details. In contrast, the seven traditional methods exhibit severe artifacts, while the Deep-SLR method appears overly smooth with limited details and a few artifacts, and DDPM-MRI also introduces additional Gaussian noise.

Table 2. Ablation Study on the NYU dataset with 4 ×, 6 × and 8 × acceleration.

Acceleration	**4 ×**			**6 ×**			**8 ×**		
Metric	**PSNR**	**SSIM**	**nRMSE**	**PSNR**	**SSIM**	**nRMSE**	**PSNR**	**SSIM**	**nRMSE**
w/o **IUM**	29.82	0.7907	0.1289	27.89	0.7239	0.1608	26.70	0.6913	0.1841
w/o **SMUM**	33.42	0.8557	0.0988	30.89	0.7904	0.1156	28.90	0.7538	0.1446
BPDM-PMRI	**34.38**	**0.891**	**0.0780**	**31.33**	**0.8210**	**0.0944**	**29.23**	**0.7741**	**0.1395**

Ablation Study To evaluate the effectiveness of BPDM-PMRI, we replace the Image Update Module (**IUM**) and Sensitivity Maps Update Module (**SMUM**) as under-sampled MR images x_t and the initial estimated sensitive maps S_t respectively for comparison. The performance comparison using 1D random masks at 4×, 6×, and 8× accelerations is presented in Table 2. It is evident that both modules contribute to enhancing the reconstruction quality. In addition, the **IUM** can improve the accuracy of the algorithm to a greater extent.

4 Conclusion

We proposed a novel blind proximal diffusion model for the joint optimization of image and sensitivity maps in parallel MRI reconstruction. Extensive experimental results highlight the superior efficiency and generalizability of BPDM-PMRI in comparison to other competitive methods.

Acknowledgments. This work was supported in part by the Key R&D Program 2022YFA1004201, in part by the Key R&D Program of Shaanxi Province under Grant 2021LL-JB-06HZ02, in part by the NSFC project under Grant U21A6005, Grant 12226007.

Disclosure of Interests. The authors have no competing interests to declare that are relevant to the content of this article.

References

1. Aggarwal, H.K., Mani, M.P., Jacob, M.: Modl: Model-based deep learning architecture for inverse problems. IEEE Trans. Med. Imaging **38**(2), 394–405 (2018)
2. Beatty, P.J., King, K.F., Marinelli, L., Hardy, C.J., Lustig, M.: Sequential application of parallel imaging and compressed sensing. In: Proc Intl Soc Mag Reson Med. vol. 17, p. 2824 (2009)
3. Block, K.T., Uecker, M., Frahm, J.: Undersampled radial mri with multiple coils. iterative image reconstruction using a total variation constraint. Magn. Reson. Med. **57**(6), 1086–1098 (2007)
4. Bolte, J., Sabach, S., Teboulle, M.: Proximal alternating linearized minimization for nonconvex and nonsmooth problems. Math. Program. **146**(1-2), 459–494 (2014)
5. Chen, C., Li, Y., Huang, J.: Calibrationless parallel mri with joint total variation regularization. In: MICCAI 2013 (2013)
6. Chen, Y., Xiao, T., Li, C., Liu, Q., Wang, S.: Model-based convolutional de-aliasing network learning for parallel mr imaging. In: -MICCAI 2019. pp. 30–38. Springer (2019)
7. Chung, H., Ye, J.C.: Score-based diffusion models for accelerated mri. Med. Image Anal. **80**, 102479 (2022)
8. Griswold, M.A., Jakob, P.M., Heidemann, R.M., Nittka, M., Jellus, V., Wang, J., Kiefer, B., Haase, A.: Generalized autocalibrating partially parallel acquisitions (grappa). Magn. Reson. Med. **47**(6), 1202–1210 (2002)
9. Haldar, J.P.: Autocalibrated loraks for fast constrained mri reconstruction. In: ISBI 2015. pp. 910–913. IEEE (2015)

10. Haldar, J.P., Zhuo, J.: P-loraks: low-rank modeling of local k-space neighborhoods with parallel imaging data. Magn. Reson. Med. **75**(4), 1499–1514 (2016)
11. Hammernik, K., Klatzer, T., Kobler, E., Recht, M.P., Sodickson, D.K., Pock, T., Knoll, F.: Learning a variational network for reconstruction of accelerated mri data. Magn. Reson. Med. **79**(6), 3055–3071 (2018)
12. Ho, J., Jain, A., Abbeel, P.: Denoising diffusion probabilistic models. NeurIPS 2020 **33**, 6840–6851 (2020)
13. Holme, H.C.M., Rosenzweig, S., Ong, F., Wilke, R.N., Lustig, M., Uecker, M.: Enlive: an efficient nonlinear method for calibrationless and robust parallel imaging. Sci. Rep. **9**(1), 3034 (2019)
14. Jin, K.H., Lee, D., Ye, J.C.: A general framework for compressed sensing and parallel mri using annihilating filter based low-rank hankel matrix. IEEE Trans. Comput. Imaging **2**(4), 480–495 (2016)
15. Liang, D., Liu, B., Wang, J., Ying, L.: Accelerating sense using compressed sensing. Magn. Reson. Med. **62**(6), 1574–1584 (2009)
16. Lustig, M., Donoho, D., Pauly, J.M.: Sparse mri: The application of compressed sensing for rapid mr imaging. Magn. Reson. Med. **58**(6), 1182–1195 (2007)
17. Lustig, M., Pauly, J.M.: Spirit: iterative self-consistent parallel imaging reconstruction from arbitrary k-space. Magn. Reson. Med. **64**(2), 457–471 (2010)
18. Pruessmann, K.P., Weiger, M., Scheidegger, M.B., Boesiger, P.: Sense: sensitivity encoding for fast mri. Magn. Reson. Med. **42**(5), 952–962 (1999)
19. Schlemper, J., Caballero, J., Hajnal, J.V., Price, A.N., Rueckert, D.: A deep cascade of convolutional neural networks for dynamic mr image reconstruction. IEEE Trans. Med. Imaging **37**(2), 491–503 (2017)
20. Song, J., Meng, C., Ermon, S.: Denoising diffusion implicit models. arXiv preprint arXiv:2010.02502 (2020)
21. Trzasko, J.D., Manduca, A.: Calibrationless parallel mri using clear. In: ASILOMAR 2011. pp. 75–79. IEEE (2011)
22. Uecker, M., Lai, P., Murphy, M.J., Virtue, P., Elad, M., Pauly, J.M., Vasanawala, S.S., Lustig, M.: Espiritan eigenvalue approach to autocalibrating parallel mri: where sense meets grappa. Magn. Reson. Med. **71**(3), 990–1001 (2014)
23. Wang, S., Tan, S., Gao, Y., Liu, Q., Ying, L., Xiao, T., Liu, Y., Liu, X., Zheng, H., Liang, D.: Learning joint-sparse codes for calibration-free parallel mr imaging. IEEE Trans. Med. Imaging **37**(1), 251–261 (2017)
24. Yang, Y., Wang, Y., Wang, J., Sun, J., Xu, Z.: An unrolled implicit regularization network for joint image and sensitivity estimation in parallel mr imaging with convergence guarantee. SIAM J. Imaging Sci. **16**(3), 1791–1824 (2023)
25. Zhang, P., Wang, F., Xu, W., Li, Y.: Multi-channel generative adversarial network for parallel magnetic resonance image reconstruction in k-space. In: MICCAI 2018. pp. 180–188. Springer (2018)